Water Oxidation

Deutsche Ausgabe: DOI: 10.1002/ange.201605666
Internationale Ausgabe: DOI: 10.1002/anie.201605666

Thin Heterojunctions and Spatially Separated Cocatalysts To Simultaneously Reduce Bulk and Surface Recombination in Photocatalysts

*Ang Li, Xiaoxia Chang, Zhiqi Huang, Chengcheng Li, Yijia Wei, Lei Zhang, Tuo Wang, and Jinlong Gong**

Abstract: *Efficient charge separation and light absorption are crucial for solar energy conversion over solid photocatalysts. This paper describes the construction of $Pt@TiO_2@In_2O_3@MnO_x$ mesoporous hollow spheres (PTIM-MSs) for highly efficient photocatalytic oxidation. TiO_2–In_2O_3 double-layered shells were selectively decorated with Pt nanoparticles and MnO_x on the inner and outer surfaces, respectively. The spatially separated cocatalysts drive electrons and holes near the surface to flow in opposite directions, while the thin heterogeneous shell separates the charges generated in the bulk phase. The synergy between the thin heterojunctions and the spatially separated cocatalysts can simultaneously reduce bulk and surface/subsurface recombination. In_2O_3 also serves as a sensitizer to enhance light absorption. The PTIM-MSs exhibit high photocatalytic activity for both water and alcohol oxidation.*

Photocatalytic reactions present a promising solution to energy- and environment-related issues.[1] For instance, water oxidation driven by solar energy has long been considered as the bottleneck of the whole solar water-splitting process.[1a,2] Light-assisted oxidation has also been widely used for the synthesis of valuable chemicals (aldehydes and ketones)[1b] under mild and environmentally friendly conditions.[1c] Thus the exploration of highly active photooxidation catalysts is significant for the development of alternative energy sources and green chemistry.

Since the seminal work by Fujishima and Honda in 1972, TiO_2 has been regarded as a benchmark photocatalyst owing to its nontoxicity, low cost, and chemical stability.[3] However, when used as a photooxidation catalyst, bare TiO_2 suffers from several problems: 1) The large band-gap energy limits its light absorption to the UV region, which accounts for only a small fraction of the total solar spectrum.[4] This can be improved by decorating the material with narrow-band-gap semiconductors that function as sensitizers.[5] 2) Severe recombination of photoinduced charges is observed. Various approaches have been reported to improve charge separation. The construction of a heterojunction is an effective method.[6] Heterojunctions can be formed between two kinds of semiconductors with staggered band structures. For instance, Liu[7] and co-workers have constructed an In_2O_3/TiO_2 heterojunction, and observed enhanced charge separation. However, charges separated by the heterogeneous interface would still suffer from severe recombination when transferred to the surface if their diffusion length is smaller than the depth of the heterojunction.[7,8] Thus the distance between surface and interface should be decreased. Alternatively, different kinds of cocatalysts can serve as electron (or hole) traps to promote charge separation.[9] Nevertheless, the simple addition of cocatalysts with a random distribution may increase the possibility of recombination and lead to severe back reactions.[9b] To solve this problem, spatial separation of the oxidation and reduction cocatalysts has been proposed by several research groups.[9a,c] However, with these cocatalysts, only surface separation can be improved effectively. Recombination in the bulk phase cannot be suppressed by cocatalysts, as evidenced by time-resolved photoluminescence (PL) measurements.[10] Thus carefully designed catalysts that simultaneously reduce bulk and surface recombination are urgently needed.

Herein, we describe the design and synthesis of $Pt@TiO_2@In_2O_3@MnO_x$ mesoporous hollow spheres (PTIM-MSs; Figure 1), which combine the advantages of spatially

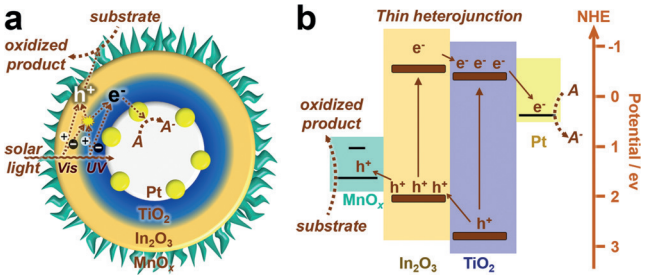

Figure 1. The PTIM-MS structure and the mechanism for photocatalytic oxidation. Pt and MnO_x are spatially separated by the TiO_2–In_2O_3 heterogeneous double-layered shell. a) The reaction process. A represents an electron acceptor; here, $NaIO_3$ was used. b) Simplified band structure of the catalyst. The CB positions of In_2O_3 and TiO_2 are −0.63 and −0.40 eV versus NHE, and the VB positions of In_2O_3 and TiO_2 were calculated to be 2.17 and 2.80 eV versus NHE according to the corresponding band gaps.

[*] A. Li, X. Chang, Z. Huang, C. Li, Y. Wei, Dr. L. Zhang, Dr. T. Wang, Prof. Dr. J. Gong
Key Laboratory for Green Chemical Technology of Ministry of Education, School of Chemical Engineering and Technology
Collaborative Innovation Center of Chemical Science and Engineering, Tianjin University
Weijin Road 92, Tianjin, 300072 (China)
E-mail: jlgong@tju.edu.cn
Supporting information and the ORCID identification numbers for the authors of this article can be found under http://dx.doi.org/10.1002/anie.201605666.

separated cocatalysts (Pt and MnO_x) and thin heterojunctions (TiO_2@In_2O_3 shell) to simultaneously reduce bulk and surface recombination. Spatially separated cocatalysts drive electrons and holes near the surface to flow in opposite directions, reducing their recombination. Thin heterojunctions can effectively separate charges in the bulk phase and enable their transfer to the surface/subsurface region where they can be easily trapped by cocatalysts for surface reactions. Furthermore, In_2O_3 serves as a sensitizer to enhance light absorption (see the Supporting Information, Figure S1). In combination with other advantages, such as a large surface area, long light-scattering path,[9a] and surface reaction kinetics promoted by cocatalysts, the PTIM-MS system is an excellent photocatalyst of both water oxidation and selective benzyl alcohol oxidation.

A hard-templating method was used to synthesize the PTIM-MSs. The synthetic process begins with SiO_2 nanospheres with Pt anchored on the external surfaces and is illustrated in the Supporting Information (Figure S2 a, f; these also include transmission electron microscope (TEM) images). SiO_2-Pt@TiO_2 (SPT; Figure S2 b, g), SiO_2-Pt@TiO_2@In_2O_3 (SPTI), and SiO_2-Pt@TiO_2@In_2O_3@SiO_2 (SPTIS, Figure S2 c, h; the outermost SiO_2 layer functions as a protective layer) were then formed successively. Subsequently, the SiO_2 core and protective layer were removed by NaOH etching at 70 °C for 8 h to form Pt@TiO_2@In_2O_3 mesoporous hollow spheres (PTI-MSs; Figure S2 d, i). Finally, MnO_x was selectively deposited on the outer surface of the PTI-MSs by a selective photodeposition method (Figure S3) to form PTIM-MSs (Figure S2 e, j). A protective layer was necessary to prevent the destruction of the thin shells during synthesis (Figures S2 i and S4 a). The primary challenge lies in the uniform coating of TiO_2 with In_2O_3. The precursors of In_2O_3 (In^{3+} ions) are difficult to adsorb to the positively charged TiO_2 surface[11] because of electrostatic repulsion.[7] Thus, without any TiO_2 surface modification, In_2O_3 will form individual nanocubes without any contact with the TiO_2 hollow spheres (Figure S4 b). To overcome this problem, sodium dodecyl sulfonate (SDS) was added as a mild sulfonating agent to modify the TiO_2 surface before the In_2O_3 coating, and a uniform In_2O_3 layer was then formed on the outer surface of the TiO_2 shells (TiO_2@In_2O_3 mesoporous hollow spheres, TI-MSs).

Figure 2 shows the evolution of the particle structure. The structure of the TI-MSs is shown in Figure 2 a–d; energy-dispersive spectroscopy (EDS) area scans confirmed that the TiO_2 hollow spheres were encapsulated by In_2O_3 shells. The structure of the SPTISs is illustrated in the high-angle annular dark field scanning transmission electron microscopy (HAADF-STEM) image in Figure 2 e, where the Pt particles can be seen as bright dots. The structure of the PTI-MSs can also be seen in the TEM and high-resolution TEM (HRTEM) images in Figure 2 f and 2 g, which confirmed the shells to be composed of two layers. The lattice spacings of the outer and inner layer are 0.293 ± 0.011 nm and 0.343 ± 0.014 nm, respectively, which are in good agreement with the (222) planes of In_2O_3 and the (101) planes of anatase TiO_2. The 0.235 ± 0.019 nm lattice spacing of dark particles inside the hollow sphere could be assigned to the (111) plane of Pt. Combined

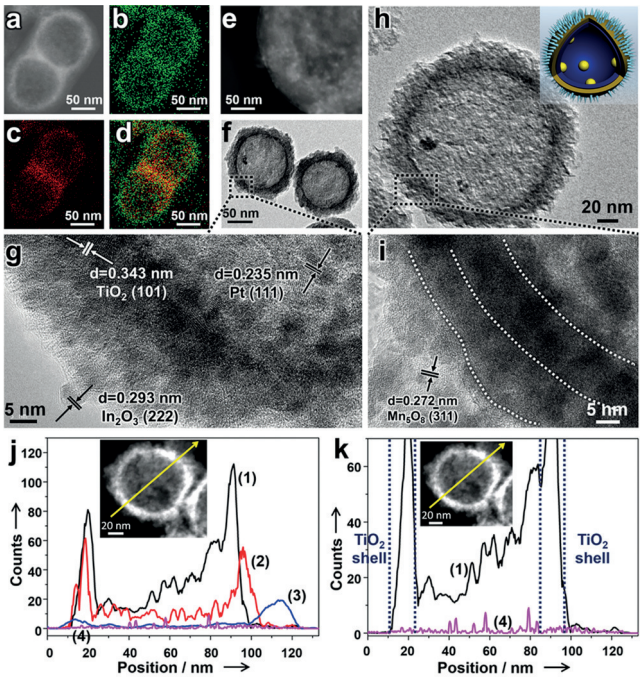

Figure 2. a–d) EDS area scans of TI-MSs. a) The HAADF-STEM image. Parts (b) and (c) show the signals of In and Ti, respectively. d) Overlay of the In and Ti signals. e) HAADF-STEM image of SPTIS. f) TEM image of PTI-MSs. The area highlighted by a dotted box is magnified in (g). g) HRTEM image of PTI-MSs. h) TEM image of PTIM-MSs. The area highlighted by a dotted box is magnified in (i). Inset: Schematic representation of the PTIM-MSs. i) HRTEM image of PTIM-MSs. j) EDS line scan of PTIM-MSs. Curves (1)–(4) refer to the signal of Ti, In, Mn, and Pt, respectively. k) Magnified EDS line scan of PTIM-MSs. The signals that are due to In and Mn are not shown.

with the EDS line scan (Figure S5 a), the PTI-MS structure has thus been unambiguously confirmed. The structure of the PTIM-MSs is displayed in Figure 2 h, i. After the addition of MnO_x, a spine-like layer appears. The lattice spacing of the spine-like layer is 0.272 ± 0.009 nm (Figure 2 i), which could be assigned to an oxide of manganese. This morphology was further confirmed by an EDS line scan through the center of an individual PTIM-MS particle (Figure 2 j, k, inset). The EDS line scan shows strong signals corresponding to Ti, In, and Mn at the edge of the nanoparticle, revealing a typical hollow structure (Figure 2 j). Every signal peak represents the position of the corresponding oxide shell. The relative shell position confirms the TiO_2@In_2O_3@MnO_x structure. The overall thickness of the heterogeneous shell is about 20 nm. In the magnified EDS line scan (Figure 2 k), the relative onset position of the Pt signal suggests that the Pt particles are distributed on the inner surface of the shell. Statistical analysis of the particle size distribution showed that the Pt particles have a uniform size distribution with an average size of 2.57 nm (Figure S5 c). Such a small size improves the dispersion of the Pt clusters.

X-ray diffraction (XRD; Figure S6 a) analysis also indicated that the shells consist of In_2O_3, TiO_2, and MnO_x, where x is between 1.0 and 2.0. The intensities of the XRD peaks corresponding to Pt were very weak owing to the low loading

(0.8 wt% by ICP).[12] The pore size and Brunauer–Emmett–Teller (BET) surface area of the PTIM-MSs were determined to be 5.3 nm (average pore size) and 288 $m^2 g^{-1}$, respectively, by nitrogen adsorption measurements (Figure S6b). These results indicate a mesoporous structure, which allows for the penetration and transportation of reactants and products.

To highlight the synergy between the thin heterojunctions and the spatially separated cocatalysts, reference catalysts, such as pure TiO_2 mesoporous hollow spheres (T-MSs; Figure S5d), pure In_2O_3 mesoporous hollow spheres (I-MSs; Figure S5e), Pt@TiO_2@MnO_x mesoporous hollow spheres (PTM-MSs),[9a] and TiO_2@In_2O_3/Pt/MnO_x mesoporous hollow spheres (TI/P/M-MSs; Figure S5b), were synthesized by similar methods. For instance, TI/P/M-MSs were synthesized by directly impregnating TI-MSs in H_2PtCl_6 and $MnSO_4$ solutions to form a hollow sphere with Pt and MnO_x distributed randomly on both the inner and outer surfaces.

Charge recombination can be analyzed by PL spectroscopy;[13] catalyst excitation with monochromatic light leads to photoluminescence as a result of the recombination of photogenerated charges. Figure 3a shows that T-MSs and I-MSs exhibit strong fluorescence, indicating severe charge recombination.[13] However, the intensity of the TI-MS fluorescence is weakened upon formation of thin heterojunctions between TiO_2 and In_2O_3 because of the inhibition of charge recombination. The PL intensity further decreased upon addition of suitable cocatalysts (Pt and MnO_x). The critical role of spatially separated cocatalysts in directing the charge carrier pathways was further confirmed by the fact that TI/P/M-MSs (Figure 3a, curve 3) with randomly distributed cocatalysts showed a much higher PL intensity than PTIM-MSs. It should be noted that compared with PTM-MSs, the PL intensity of the PTIM-MSs is weaker, indicating the efficient synergy between thin heterojunctions and spatially separated cocatalysts, which will be further discussed below.

When used in photooxidation reactions, the PTIM-MSs exhibited high activity for both water oxidation (Figure 3b) and selective benzyl alcohol oxidation (Figure 3c,d).[14] The O_2 evolution rate (466.6 $\mu mol\, g^{-1} h^{-1}$) was higher than for conventional TiO_2-based catalysts without decoration (typically 67–180 $\mu mol\, g^{-1} h^{-1}$).[9a,15] For benzyl alcohol oxidation, the apparent quantum efficiency (AQE) reached 49.2% and 24.2% under UV (254 nm) and visible (435 nm) irradiation, which is also higher than that of bare TiO_2 (typically 17%–39% under UV light and 4.3%–20% under visible light).[16] Notably, the photooxidation activity of the catalysts decreased in the same order as the PL intensity increased (activity: PTIM-MSs > PTM-MSs > TI/P/M-MSs > PTI-MSs > TI-MSs > T-MSs or I-MSs). Their activity in photocatalytic oxidation was obviously increased by the reduction of charge recombination and improved light absorption.

To further investigate the synergy between the thin heterojunctions and the spatially separated cocatalysts, time-resolved PL spectroscopy was employed to monitor the fluorescence decay. Samples with efficient charge separation would show slow PL decay owing to the long lifetimes of the electrons and holes.[17] The decay curves were obtained by fitting the observed data (the dots in Figure 4a) according to the extended exponential function[18]

$$I = I_0 t^{\beta-1} \exp\left\{-\left(\frac{t}{\tau}\right)^{\beta}\right\}$$

where τ (lifetime) and β (shape factor) are parameters to be fitted, and I_0 is the initial intensity. I and t refer to the instantaneous intensity and time, respectively. Table 1 summarizes the τ and β values of different catalysts.[19] As shown in Figure 4a and Table 1, the T-MSs showed fast PL decay, whereas the decay time was prolonged when the cocatalysts were separately loaded (PTM-MSs). The decay time of the PTIM-MSs is even longer owing to the further reduction of bulk recombination, which is caused by the heterojunction between TiO_2 and In_2O_3.

To investigate the charge recombination in the bulk phase and the surface region separately, the catalysts were subjected to time-resolved PL

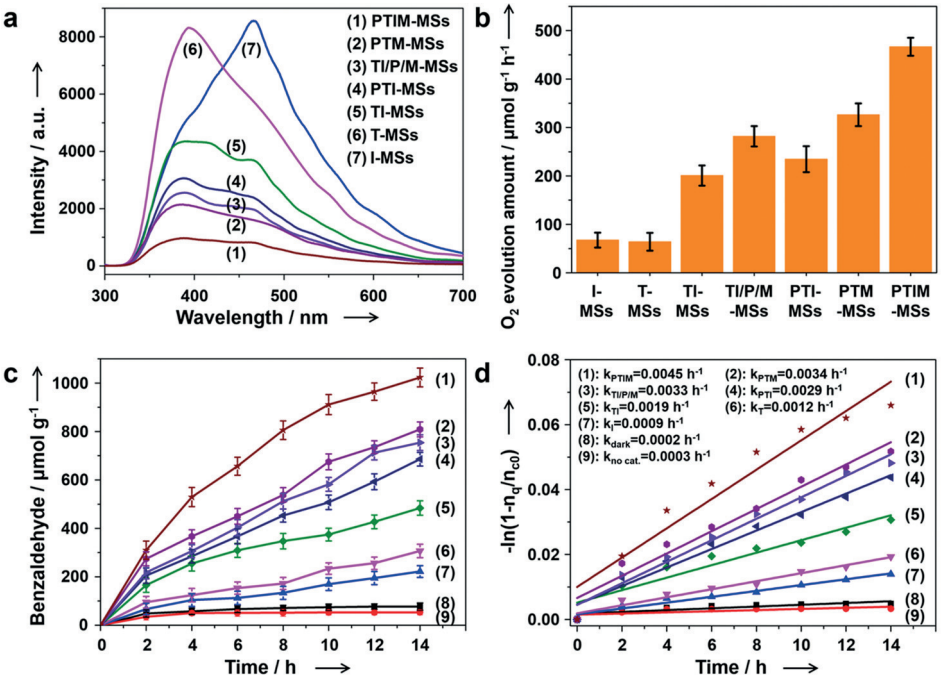

Figure 3. a) PL spectra (λ_{ex} = 260 nm) of the catalysts. b) The activity of the various photocatalysts (0.06 g) in water oxidation under simulated sunlight irradiation (UV/Vis irradiation). c) The activity of the various photocatalysts in alcohol oxidation under simulated sunlight irradiation. d) The corresponding kinetics. Traces (1)–(9) in Figure (c) and (d) refer to PTIM-MSs, PTM-MSs, TI/P/M-MSs, PTI-MSs, TI-MSs, T-MSs., I-MSs, and PTM-MSs under dark conditions and no catalyst, respectively. Traces (1)–(7) and (9) were obtained under simulated sunlight irradiation. Catalyst amount: 0.06 g.

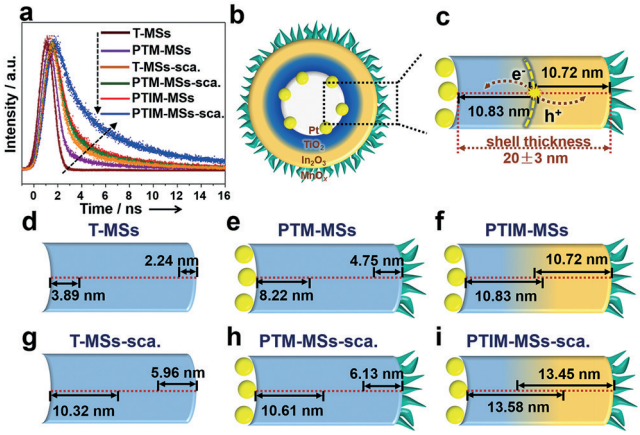

Figure 4. a) Time-resolved PL spectra of T-MSs, PTM-MSs, and PTIM-MSs. Catalysts in scavenger solutions are denoted by -sca. The samples were excited at 355 nm, and the photoluminescence was monitored at 480 nm. Observed data points are indicated by dots, while the fits are shown as smooth curves. b) PTIM-MSs. c) The average shell thickness and the synergy between the thin heterojunctions and the spatially separated spatial cocatalysts. d–f) Nominal diffusion lengths of the catalysts without scavengers. g–i) Nominal diffusion lengths of the catalysts in the presence of scavengers.

Table 1: Fitting of the time-resolved PL spectra of the catalysts in the presence and absence of scavengers and the nominal charge diffusion lengths.

Catalyst[a]	τ[b] [ns]	β[c]	$L_{n\text{-}TiO_2}$[d] [nm]	$L_{n\text{-}TiO_2}$[e] [nm]	$L_{p\text{-}In_2O_3}$[f] [nm]
T-MSs	0.42	1.10	3.89	2.24	3.85
T-MSs-sca.	2.96	3.37	10.32	5.96	10.21
PTM-MSs	1.88	1.04	8.22	4.75	8.14
PTM-MSs-sca.	3.13	3.03	10.61	6.13	10.50
PTIM-MSs	3.26	2.99	10.83	6.25	10.72
PTIM-MSs-sca.	5.13	1.96	13.58	7.84	13.45

[a] Catalysts in scavenger solutions are denoted by -sca. The scavenger solutions were prepared by dissolving 0.9 g $NaIO_3$ and 3 mL butanol in 18 mL deionized water. [b] Charge lifetime. [c] Shape factor. [d] Nominal diffusion length of electrons in polycrystalline TiO_2. [e] Nominal diffusion length of holes in polycrystalline TiO_2. [f] Nominal diffusion length of holes in polycrystalline In_2O_3.

analysis in a mixed $NaIO_3$ (e^- scavenger) and butanol (h^+ scavenger) solution.[9c,20] The scavengers can greatly promote the surface reactions, leading to the rapid consumption of charges on the surface, inhibiting surface recombination and quenching the surface fluorescence.[21] Whereas it has been shown that charge transfer from a nanoparticle (ca. 20 nm) to its surface occurs on the picosecond timescale for a TiO_2 film,[2] the transportation time will be prolonged to the nanosecond timescale for our sintered TiO_2 powder as the numerous interfaces in polycrystalline shells act as recombination centers and obstacles for charge movement.[18,19] Thus, in the scavenger solution, the fluorescence decay on the nanosecond timescale is mainly caused by bulk recombination. Catalysts in scavenger solutions are denoted as -sca. As shown in Figure 4a and Table 1, the decay times for PTM-MSs are very similar in the absence and presence of the scavengers, and very close to that of T-MSs-sca., indicating that spatially separated cocatalysts cannot suppress the recombination of charges in the bulk phase. However, for PTIM-MSs-sca., the decay time is obviously longer than for either PTM-MSs-sca. or T-MSs-sca., suggesting effective electron and hole separation in the bulk phase of the PTIM-MSs.

The nominal diffusion lengths of the electrons and holes were calculated using a widely used method according to the lifetime and mobility of charges (see the Supporting Information).[10,22] Although longer diffusion lengths have been reported for crystalline TiO_2 films,[22c] nanometer diffusion lengths are normal for sintered TiO_2 powder as the numerous interfaces in the polycrystalline shells act as recombination centers and obstacles for charge movement.[19] The addition of cocatalysts can increase the nominal charge diffusion length to some extent while electrons and holes deep in the bulk phase still cannot migrate to the surface (Figure 4e,h). However, when a heterogeneous interface between TiO_2 and In_2O_3 is constructed in shells, the nominal diffusion length increases greatly. Combined with the thinness of the heterogeneous shell, charges generated deeply in the bulk phase can be transferred to the surface/subsurface region and are easily trapped by the cocatalysts (Figure 4c). Thus, for PTIM-MSs, charges generated in both the bulk and surface/subsurface regions can migrate to the corresponding cocatalysts (Figure 4f,i) and take part in redox reactions, greatly enhancing the separation efficiency.

In summary, we have described the synthesis of PTIM-MSs catalysts with Pt particles and MnO_x on the inner and outer surfaces of TiO_2–In_2O_3 thin heterogeneous double-layered mesoporous hollow spheres. Owing to the synergy between the thin heterojunctions and spatially separated cocatalysts, charge recombination in both bulk and surface/subsurface regions can be efficiently reduced. Furthermore, In_2O_3 extends the absorption spectrum of TiO_2 to the visible region (up to ca. 510 nm). In view of the enhanced light absorption, charge separation, and surface reaction, the PTIM-MS structure can provide inspiration for other photocatalytic systems, for example, for light-assisted CO_2 reduction.

Acknowledgements

We thank the National Key Projects for Fundamental Research and Development of China (2016YFB0600900), the National Natural Science Foundation of China (U1463205, 21525626, 51302185), the Specialized Research Fund for the Doctoral Program of Higher Education (20120032110024, 20130032120018), the Scientific Research Foundation for the Returned Overseas Chinese Scholars (MoE), and the Program of Introducing Talents of Discipline to Universities (B06006) for financial support.

Keywords: charge recombination · heterojunctions · mesoporous materials · solar energy conversion · water oxidation

How to cite: *Angew. Chem. Int. Ed.* **2016**, *55*, 13734–13738
Angew. Chem. **2016**, *128*, 13938–13942

[1] a) X. Sala, I. Romero, M. Rodríguez, L. Escriche, A. Llobet, *Angew. Chem. Int. Ed.* **2009**, *48*, 2842; *Angew. Chem.* **2009**, *121*, 2882; b) A. Tanaka, K. Hashimoto, H. Kominami, *J. Am. Chem. Soc.* **2012**, *134*, 14526; c) J. C. Colmenares, R. Luque, *Chem. Soc. Rev.* **2014**, *43*, 765.
[2] J. Tang, J. R. Durrant, D. R. Klug, *J. Am. Chem. Soc.* **2008**, *130*, 13885.
[3] A. Fujishima, K. Honda, *Nature* **1972**, *238*, 37.
[4] A. Li, P. Zhang, X. Chang, W. Cai, T. Wang, J. Gong, *Small* **2015**, *11*, 1892.
[5] a) J. Lv, T. Kako, Z. Li, Z. Zou, J. Ye, *J. Phys. Chem. C* **2010**, *114*, 6157; b) Z. Wang, B. Huang, Y. Dai, X. Qin, X. Zhang, P. Wang, H. Liu, J. Yu, *J. Phys. Chem. C* **2009**, *113*, 4612.
[6] a) Y. Zheng, L. Lin, B. Wang, X. Wang, *Angew. Chem. Int. Ed.* **2015**, *54*, 12868; *Angew. Chem.* **2015**, *127*, 13060; b) H. Wang, L. Zhang, Z. Chen, J. Hu, S. Li, Z. Wang, J. Liu, X. Wang, *Chem. Soc. Rev.* **2014**, *43*, 5234; c) X. Liu, S. Inagaki, J. Gong, *Angew. Chem. Int. Ed.* **2016**, DOI: 10.1002/anie.201600395; *Angew. Chem.* **2016**, DOI: 10.1002/ange.201600395.
[7] J. Mu, B. Chen, M. Zhang, Z. Guo, P. Zhang, Z. Zhang, Y. Sun, C. Shao, Y. Liu, *ACS Appl. Mater. Interfaces* **2012**, *4*, 424.
[8] C. Li, S. Wang, T. Wang, Y. Wei, P. Zhang, J. Gong, *Small* **2014**, *10*, 2783.
[9] a) A. Li, T. Wang, X. Chang, W. Cai, P. Zhang, J. Zhang, J. Gong, *Chem. Sci.* **2016**, *7*, 890; b) S. Obregón, G. Colón, *Appl. Catal. B* **2014**, *144*, 775; c) R. Li, F. Zhang, D. Wang, J. Yang, M. Li, J. Zhu, X. Zhou, H. Han, C. Li, *Nat. Commun.* **2013**, *4*, 1432.
[10] a) S. D. Stranks, G. E. Eperon, G. Grancini, C. Menelaou, M. J. Alcocer, T. Leijtens, L. M. Herz, A. Petrozza, H. J. Snaith, *Science* **2013**, *342*, 341; b) A. C. Arango, L. R. Johnson, V. N. Bliznyuk, Z. Schlesinger, S. A. Carter, H.-H. Hörhold, *Adv. Mater.* **2000**, *12*, 1689; c) G. E. Eperon, S. D. Stranks, C. Menelaou, M. B. Johnston, L. M. Herz, H. J. Snaith, *Energy Environ. Sci.* **2014**, *7*, 982.
[11] M. S. Vohra, S. Kim, W. Choi, *J. Photochem. Photobiol. A* **2003**, *160*, 55.
[12] a) F. Jiang, L. Zeng, S. Li, G. Liu, S. Wang, J. Gong, *ACS Catal.* **2015**, *5*, 438; b) T. Wang, F. Jiang, G. Liu, L. Zeng, Z. Zhao, J. Gong, *AlChE J.* **2016**, DOI: 10.1002/aic.15339.
[13] C. Li, P. Zhang, R. Lv, J. Lu, T. Wang, S. Wang, H. Wang, J. Gong, *Small* **2013**, *9*, 3951.
[14] Z. Huang, Y. Liu, Q. Zhang, X. Chang, A. Li, L. Deng, C. Yi, Y. Yang, N. M. Khashab, J. Gong, Z. Nie, *Nat. Commun.* **2016**, *7*, 12147.
[15] a) T. Han, Y. Chen, G. Tian, J.-Q. Wang, Z. Ren, W. Zhou, H. Fu, *Nanoscale* **2015**, *7*, 15924; b) M. Ni, M. K. Leung, D. Y. Leung, K. Sumathy, *Renewable Sustainable Energy Rev.* **2007**, *11*, 401; c) J. Schneider, M. Matsuoka, M. Takeuchi, J. Zhang, Y. Horiuchi, M. Anpo, D. W. Bahnemann, *Chem. Rev.* **2014**, *114*, 9919.
[16] a) S. Higashimoto, N. Kitao, N. Yoshida, T. Sakura, M. Azuma, H. Ohue, Y. Sakata, *J. Catal.* **2009**, *266*, 279; b) Y. Sugano, Y. Shiraishi, D. Tsukamoto, S. Ichikawa, S. Tanaka, T. Hirai, *Angew. Chem. Int. Ed.* **2013**, *52*, 5295; *Angew. Chem.* **2013**, *125*, 5403; c) D. Tsukamoto, Y. Shiraishi, Y. Sugano, S. Ichikawa, S. Tanaka, T. Hirai, *J. Am. Chem. Soc.* **2012**, *134*, 6309; d) L. Liu, S. Ouyang, J. Ye, *Angew. Chem. Int. Ed.* **2013**, *52*, 6689; *Angew. Chem.* **2013**, *125*, 6821.
[17] J. Zhang, M. Zhang, R.-Q. Sun, X. Wang, *Angew. Chem. Int. Ed.* **2012**, *51*, 10145; *Angew. Chem.* **2012**, *124*, 10292.
[18] K. Fujihara, S. Izumi, T. Ohno, M. Matsumura, *J. Photochem. Photobiol. A* **2000**, *132*, 99.
[19] P. Salvador, *J. Appl. Phys.* **1984**, *55*, 2977.
[20] Y. Inel, D. Ertek, *J. Chem. Soc. Faraday Trans.* **1993**, *89*, 129.
[21] a) I. S. Cho, H. S. Han, M. Logar, J. Park, X. Zheng, *Adv. Energy Mater.* **2016**, *6*, 1501840; b) X. Chang, T. Wang, P. Zhang, J. Zhang, A. Li, J. Gong, *J. Am. Chem. Soc.* **2015**, *137*, 8356.
[22] a) J. De Wit, G. Van Unen, M. Lahey, *J. Phys. Chem. Solids* **1977**, *38*, 819; b) Q. Dong, Y. Fang, Y. Shao, P. Mulligan, J. Qiu, L. Cao, J. Huang, *Science* **2015**, *347*, 967; c) L. Peter, *J. Phys. Chem. C* **2007**, *111*, 6601.

Received: June 11, 2016
Revised: July 6, 2016
Published online: July 22, 2016

